Correspondence

Sampling on Concentric Circles

Nikolaos E. Myridis and Christodoulos Chamzas*

***Abstract*— Two forms of a sampling theorem for concentric circles are established for a bandlimited two-dimensional (2-D) function. The location of the samples is prescribed either on equidistant circles or on the roots of the Bessel function $J_0(\,)$. Both methods give comparable results, however, the number of samples required for their numerical evaluation is significantly less for the root-sampling formulation.**

***Index Terms*—Bessel functions, interpolation, reconstruction, 2-D-polar sampling**

I. Introduction

Two-dimensional (2-D) sampling is a common procedure for many applications, such as biomedical imaging, astronomy, radar, crystallography, etc. In these fields there is a variety of sampling schemes, adequate to different imaging methods respectively. Magnetic resonance imaging (MRI) is a representative example of this kind. Although an exact treatment of any kind of arbitrary rectangular sampling [1] has been established in the multidimensional signal processing, more sophisticated nonrectangular sampling orientations have not been explored.

Polar sampling offers some useful advantages in MRI. We refer, for instance, to projection reconstruction (PR) methods which use polar trajectories in k-space (Fourier domain). PR has insensitivity to motion artifacts since it does not use phase data extensively. The latter is very important for brain pulsatility imaging [2], thoracic or abdominal imaging, etc. Moreover, polar sampling introduces a better description of low frequencies in contrast to rectangular sampling. Indeed, polar trajectories give a redundant collection of data near the origin where the spectral content is significant.

However, reconstruction from polar samples produces visible artifacts. This is due to the interpolation required for the conversion to the rectangular sampling geometry [3]. In order to reduce these artifacts [4], the Hankel transform (HT) was proposed. In this work, we study an alternative method [5].

We present in this essay two forms of a sampling theorem for polar geometry. In the first case, the values of the bandlimited function are located on equidistant circles, where in the second case, the radii of the sampling circles are located on the zeros of the Bessel function $J_0(\,)$. The first form is a simple application of the Radon transform [6], while the second one is new and it was only known for a specific class of functions, the circularly symmetric ones [7, p. 163]. Here, the applicability of the second one is extended to arbitrary functions. In comparison to the uniform polar sampling of the first form, the 2-D sampling on roots appears to possess an advantage, which improves the reconstruction from a finite number of samples. Simulation results enlighten the polar sampling theorem and indicate its usefulness.

Manuscript received January 8, 1996; revised October 1, 1997. The Associate Editor responsible for coordinating the review of this paper and recommending its publication was M. W. Vannier. *Asterisk indicates corresponding author.*

N. E. Myridis is with the Department of Electrical Engineering and Computer Science, Democritus University of Thrace, Xanthi 67100 Greece

*C. Chamzas is with the Department of Electrical Engineering and Computer Science, Democritus University of Thrace, Xanthi 67100 Greece (e-mail: chamzas@voreas.ee.duth.gr).

Publisher Item Identifier S 0278-0062(98)04890-3.

II. Uniform Polar Sampling

We consider a 2-D function, namely, $f(r,\theta)$, with 2-D Fourier transform (FT)

$$f(r,\theta) \leftrightarrow F(\omega,\varphi) \tag{1}$$

where (r,θ) and (ω,φ) stand for the polar coordinates in the spatial and Fourier domains, respectively. The function $f(\,)$ is considered to be bandlimited, i.e.,

$$F(\omega,\varphi) = 0, (\omega,\varphi) \notin B \tag{2}$$

where B is the region of support of $F(\,)$. We can always find an α such that

$$F(\omega,\varphi) = 0, \omega > \alpha. \tag{3}$$

Such a function will be referred as α-bandlimited.

Uniform Sampling Theorem: If the values of the α-bandlimited function $f(r,\theta)$ are known on the concentric circles $f(r = ir_0,\theta)$, $r_0 \leq (\pi/\alpha)$, where r_0 is the radial sampling distance, then the function is known for every r and θ.

The proof is given in the Appendix.

Image reconstruction: If the values of an α-bandlimited function $f(r,\theta)$ are known on the concentric circles $f(r = ir_0,\theta), r_0 \leq \pi/\alpha$, then the function $f(r,\theta)$ is given from the following formula:

$$\boxed{f(r,\theta) = \sum_{n=-\infty}^{\infty} f(nr_0,\theta)\,\frac{r_0\sin(\sigma(r-nr_0))}{\pi(r-nr_0),} \quad \text{for } \alpha \leq \sigma \leq \frac{2\pi}{r_0} - \alpha} \tag{4}$$

where σ is the bandwidth of the interpolating function [7, p. 120]. A common choice of σ is α.

III. Polar Sampling on the Roots of $J_0(r)$

In the second form we assume that the values of the function are known on concentric circles located on the zeroes of $J_0(\alpha r)$, and we will express $f(r,\theta)$ by these samples.

Lemma 1: If the nth-order HT $\tilde{g}_n(\omega)$, of a circularly symmetric function $g(r)$ is α-bandlimited, i.e.,

$$g(r) \overset{h_n}{\longleftrightarrow} \tilde{g}_n(\omega) = 0, \qquad \omega > \alpha \tag{5}$$

then its zeroth-order HT is α-bandlimited too, i.e.,

$$g(r) \overset{h_0}{\longleftrightarrow} \tilde{g}_0(\omega) = 0, \qquad \omega > \alpha. \tag{6}$$

Note: h_i denotes the ith-order HT

$$g(r) \overset{h_i}{\longleftrightarrow} \tilde{g}_i(\omega) = \int_0^{\infty} rg(r)J_i(\omega r)\,dr. \tag{7}$$

The proof is given in the Appendix.

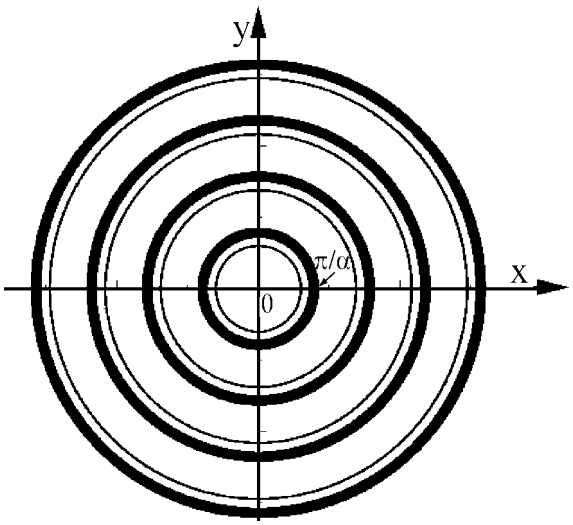

(a)

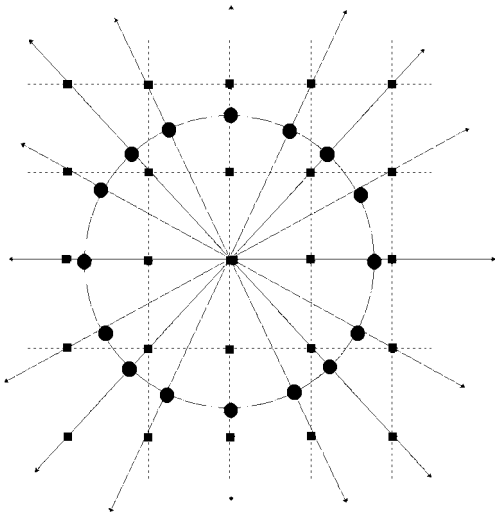

(b)

Fig. 1. (a) The space tracing: uniform sampling (thick line) and sampling on the roots of $J_0(r)$ (thin line). (b) Required number of samples/circle by a uniform sampling for a 5×5 grid.

Polar Sampling Theorem: We consider the samples of $f(r,\theta)$ on the concentric circles $r = a_i$, with a_i given by

$$J_0(a_i\alpha) = 0 \tag{8}$$

where α is the maximum spectral content for a radius as defined in (3). Then $f(r,\theta)$ can be recovered from its samples on these concentric circles [Fig. 1(a)]. In fact, we shall prove that

$$\boxed{f(r,\theta) = \frac{2}{a} \sum_{n=-\infty}^{\infty} \sum_{i=1}^{\infty} \frac{a_i b_n(a_i)}{J_1(a_i\alpha)} \frac{J_o(\alpha r)}{a_i^2 - r^2} \cdot e^{jn\theta}} \tag{9}$$

with

$$\boxed{b_n(r_0) = \frac{1}{2\pi} \int_{-\pi}^{\pi} f(r = r_0, \theta) \cdot e^{-jn\theta} \cdot d\theta} \tag{10}$$

Proof: The function $f(r,\theta)$ can be expanded into a Fourier series in θ as

$$f(r,\theta) = \sum_{n=-\infty}^{\infty} b_n(r) e^{jn\theta} \tag{11}$$

with Fourier series coefficients

$$b_n(r) = \frac{1}{2\pi} \int_{-\pi}^{\pi} f(r,\theta) e^{-jn\theta}\, d\theta. \tag{12}$$

By taking 2-D FT on both sides of (11) it can be shown that the series $\Sigma_{n=-\infty}^{\infty} \tilde{b}_{nn}(\omega) \cdot e^{-jn\varphi}$ equals to the 2-D FT $F(\omega,\varphi)$ [7], where $\tilde{b}_{nn}(\omega)$ symbolizes the nth-order HT of $b_n(r)$. Since by (3), the series is zero for $\omega > \alpha$ and every φ, it results that all the coefficients are also zero for $\omega > \alpha$. Therefore,

$$\tilde{b}_{nn}(\omega) = 0, \qquad \omega > \alpha. \tag{13}$$

From Lemma 1 we obtain

$$\tilde{b}_{n0}(\omega) = 0, \qquad \omega > \alpha \tag{14}$$

with $\tilde{b}_{n0}(\omega)$ the zero-order HT of $b_n(r)$.

Thus, the sampling theorem [7] can be applied on the coefficients $b_n(r)$, i.e.,

$$b_n(r) = \frac{2}{a} \sum_{i=1}^{\infty} \frac{a_i b_n(a_i)}{J_1(a_i\alpha)} \frac{J_0(\alpha r)}{a_i^2 - r^2}. \tag{15}$$

Combining (11) and (15), (9) results. $\therefore$

Equation (9) forms the polar sampling theorem for an arbitrary function. The regeneration of a function from its samples on the roots of $J_0(r)$ is, therefore, feasible. Notice that for $\theta = 0$ we obtain from (9) the known sampling theorem for circular symmetric 2-D functions (15) [7].

IV. Image Reconstruction

If the values of an α-bandlimited function $f(r,\theta)$ are known on the concentric circles $f(r = a_i, \theta)$, where $a_i, i = 1, 2, \cdots$, are given from $J_0(a_i\alpha) = 0$, then we can find the function $f(r,\theta)$ as follows.

Step 1) For each concentric circle $f(r = a_i, \theta)$, find the Fourier series coefficients by (12).

Step 2) Then $f(r,\theta)$ is given by (9).

NOTE: With the additional assumption, that if a 2-D function $f(r,\theta)$ is *angularly bandlimited* [8 p. 187], then its Fourier Series expansion in θ is also bandlimited, i.e., $b_n(\alpha_i) = 0$ for $n > N_i$ and (9) may be simplified to

$$f(r,\theta) = \frac{2}{\alpha} \sum_{i=1}^{\infty} \sum_{n=-N_i}^{N_i} \frac{a_i b_n(a_i)}{J_1(a_i\alpha)} \frac{J_0(\alpha r)}{a_i^2 - r^2} \cdot e^{jn\theta}. \tag{16}$$

V. Sampling Distance

The polar sampling theorem on the roots of $J_0(\,)$—(9)—implies a sampling distance. We show that this sampling distance is asymptotically the same with the uniform one.

Indeed, two consecutive samples along the variable r (circles) for the root-sampling have a distance of

$$r_s = a_{i+1} - a_i = \frac{x_{i+1} - x_i}{\alpha} \tag{17}$$

with x_i the roots of $J_0(r)$, i.e., $J_0(x_i) = 0$. The location of roots drawn from [9] is

$$J_0(x_i) = 0, \ \frac{x_i}{\pi} = i - \frac{1}{4} + \frac{0.050661}{4i-1} - \frac{0.053041}{(4i-1)^3} + \frac{0.262\,051}{(4i-1)^5} - \cdots. \tag{18}$$

For large values of i the difference of two consequent roots is

$$\Delta x_i = x_{i+1} - x_i \cong \pi\left(1 - \frac{4 \cdot 0.050661}{(4i+3)(4i-1)} \cdots\right) \leq \pi \tag{19}$$

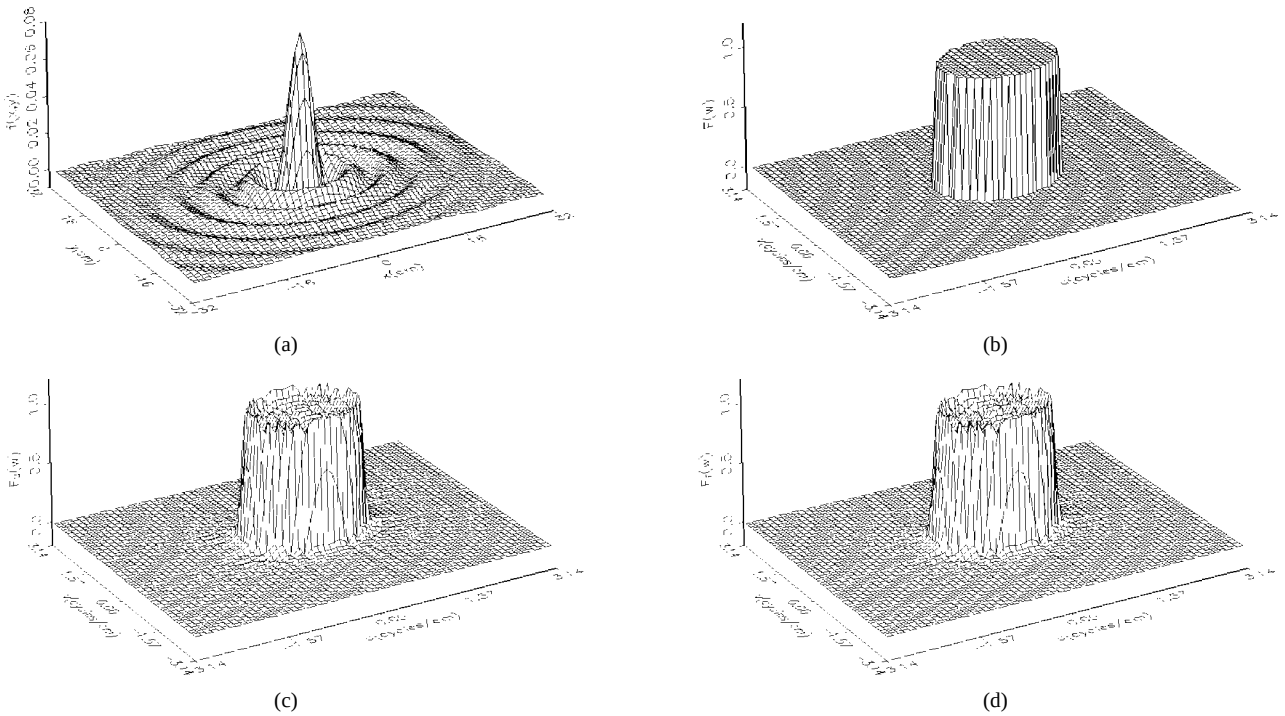

Fig. 2. (a) The first simulation function, namely, the *sombrero* one. $d = 1$. (b) The 2-D Fourier transform of the *sombrero* function, namely, the *cylinder* one. $a = 1$ cycles/cm. (c) The spectrum of the uniform polar sampling for the *somb* function. Number of circles and samples $N = 32, M = 2952$, respectively. Sampling distance $r_0 = 1$ cm. (d) The spectrum of the polar sampling on the roots of $J_0(r)$ for the somb function. Number of circles and samples $N = 32, M = 512$, respectively.

and the sampling distance results

$$r_s = \frac{\Delta x_i}{\alpha} \leq \frac{\pi}{\alpha}. \tag{20}$$

Equation (20) for large values of i gives

$$\lim_{i \to \infty} r_s = \frac{\pi}{\alpha}. \tag{21}$$

For the uniform sampling we assume a maximum radial bandwidth of α for the function $f(\,)$. This will also be the maximum frequency for a projection of its 2-D FT. According to the Nyquist theorem and the Section II, the sampling frequency must fulfill the inequality

$$\omega_0 \geq 2 \cdot \omega_{\max} \Rightarrow \omega_{0,\min} = \frac{2\pi}{r_{0,\max}} = 2 \cdot \alpha \Rightarrow r_{0,\max} = \frac{\pi}{\alpha}. \tag{22}$$

The $r_{0,\max}$ given by (22) is the maximum for all the lines passing through the origin since the maximum width for a projection was assumed. Thereafter, from (21) and (22), it follows that on the average we have the same density of samples along r for a uniform and root-sampling i.e.,

$$r_s = r_0. \tag{23}$$

VI. Numerical Evaluation

We give a brief discussion of the numerical implementation of both methods and present some examples. The final objective is to obtain the reconstructed image on a rectangular grid.

The first question we have to answer is how many concentric circles should we use? Having a finite number of concentric circles results to the well-known truncation artifacts, and they are similar for both methods. For our examples we choose $N = 32$ concentric circles.

The second question is how many samples, M, do we need on each concentric circle? For the uniform sampling, we must apply (4) for each point on the rectangular grid. As we can see from Fig. 1(b), for a rectangular grid 5×5 we need $M = 16$ samples on each concentric circle, i.e., with 16 different radii we can cover all the grid points. For a 64×64 grid the number is $M = 2952$. Actually for a $K \times K$ grid, with K large $(K > 80)$, we found that $M \cong 0.62K^2$ (*Farey sequence* [10]). For the polar sampling case, we take $M = 512$. This number was chosen since it gives a considerably denser sampling rate on the outer concentric circle of our examples, than the one predicted by the sampling theorem.

At first, we present two numerical examples. In the first example we apply the polar sampling theorem on the sombrero function [Fig. 2(a)]

$$f(r) = \frac{dJ_1(dr)}{2\pi r} \tag{24}$$

with 2-D FT being the cylinder function [Fig. 2(b)]

$$F(\omega) = \begin{cases} 1, & 0 \leq \omega < d \\ 0, & \omega > d. \end{cases} \tag{25}$$

In the first case we sampled $f(r)$ uniformly with $r_0 = 1$ cm, $d = 1$ cycles/cm. We used $r_0 = 1$ cm instead of $r_0 = \pi$ cm (oversampling) in order to reduce aliasing errors. Consequently, even if the bandwidth was $\alpha = 1$ cycles/cm we used $\alpha = \pi$ cycles/cm. We used 32 samples along the variable r, i.e., 32 circles. Then the values of the function were evaluated on 64×64 rectangular grid, using (4) with $r_0 = 1$ cm. To evaluate these 64×64 points, we need 2952 samples on each circle, a total of $32 \times 2952 = 94\,464$ samples. A 2-D FFT was performed on this rectangular array $f(r, \theta)$ and Fig. 2(c) depicts the resulting spectrum.

In the second case we sampled $f(r)$ on the roots of $J_0(r)$ (18). We considered the equal number of circles $(N = 32)$. The factors d and α were not altered. Again the values of the function $f(r, \theta)$ were evaluated on 64×64 rectangular grid. To evaluate the Fourier series coefficients we used $M = 512$ samples on each circle. Finally, a 2-D

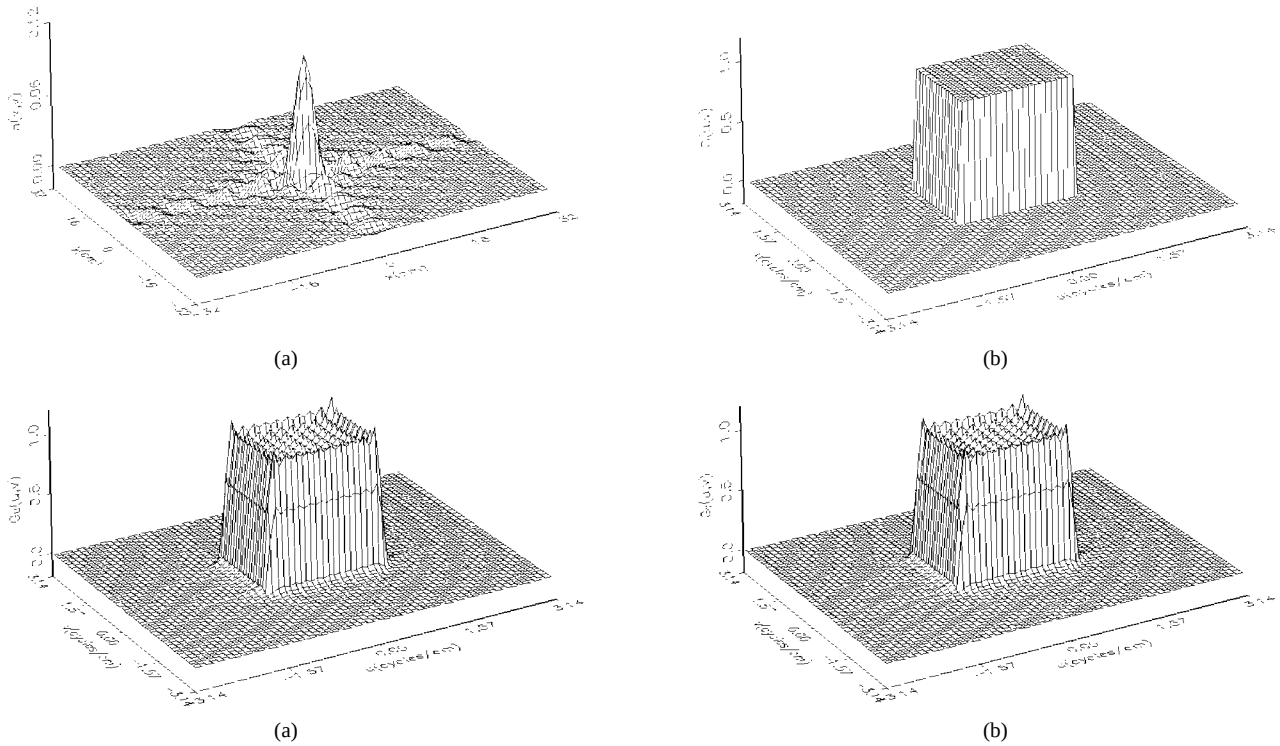

(a) (b)

(a) (b)

Fig. 3. (a) The second simulation function, namely, the *sinc* one. $a = b = 1$. (b) The 2-D FT of the *sinc* function, namely, the *rectangle* one. (c) The spectrum of the uniform polar sampling for the *sinc* function. $a = b = 1$ cycles/cm. Number of circles and samples $N = 32, M = 2952$, respectively. $r_0 = 1$ cm. (d) The spectrum of the polar sampling on the roots of $J_0(r)$ for the sinc function. $a = b = 1$ cycles/cm. $N = 32, M = 512$.

TABLE I
THE SIGNAL-TO-NOISE (S/N) RATIO OF UNIFORM AND ROOT SAMPLING FOR DIFFERENT VALUES OF M

Samples on each circle	Uniform Sampling $G_u(u,v)$		Root Sampling $G_r(u,v)$	
M	S/N (db)		S/N (db)	
	Spectrum $G(u,v)$	Spectrum $G_O(u,v)$	Spectrum $G(u,v)$	Spectrum $G_O(u,v)$
128	16.14	36.53	16.27	40.69
64	16.10	33.33	16.24	35.23
32	14.74	20.54	15.33	22.90

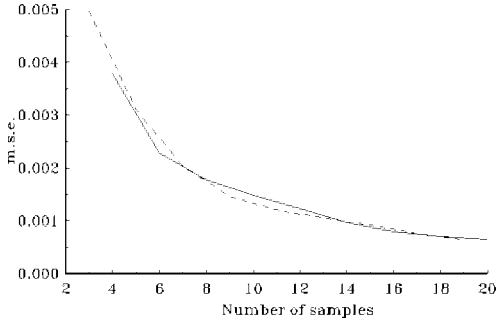

Fig. 4. The MSE of the 1-D uniform (dashed line) and root (solid line) sampling for a pulse reconstruction versus the number of samples.

FFT was performed on the 64×64 array and the obtained spectrum is illustrated in Fig. 2(d).

In the second example we used a function which is not a circular symmetric one. We assume the sinc function [Fig. 3(a)]

$$g(x,y) = ab\ \frac{\mathrm{sinc(ax,by)}}{\pi^2} = ab\ \frac{\mathrm{sinc(ax)sinc(by)}}{\pi^2} \tag{26}$$

with 2-D FT being the rectangle function [Fig. 3(b)]

$$G(u,v) = rect\left(\frac{u}{a}, \frac{v}{b}\right) = \begin{cases} 1, & |u| < a, |v| < b \\ 0, & \text{otherwise.} \end{cases} \tag{27}$$

The sampling interval in the uniform sampling is $r_0 = \pi/\sqrt{2}$ cm since $a = b = 1$ cycles/cm and, consequently, $\alpha = \sqrt{a^2 + b^2} = \sqrt{2}$. Again, in order to reduce aliasing we used $r_0 = 1$ cm (oversampling). The rest sampling parameters are those of the first case. Fig. 3(c) depicts the reconstruction achieved by the uniform sampling, i.e., the spectrum $G_u(u,v)$. Fig. 3(d) displays the reconstruction of the spectrum $G_r(u,v)$ via the root-sampling. It is important to notice that the results are almost the same but we used six times fewer samples for the root-sampling case.

In order to compare the performance of the two methods, we then assumed that we know the same number, M, of samples on each circle. For the uniform sampling the required number of samples on each circle is obtained via a discrete Fourier series interpolation, and (4) is applied. Then we evaluate the normalized root-mean-square (NRMS) error

$$\mathrm{(S/N) = 10\ log_{10}} \left(\frac{\iint\limits_{\mathrm{u,v}} |\mathrm{G(u,v)}|^2\ \mathrm{du\ dv}}{\iint\limits_{\mathrm{u,v}} |\mathrm{G_R(u,v) - G(u,v)}|^2\ \mathrm{du\ dv}} \right)$$

where $G_R(u,v)$ is the reconstructed spectrum, $G_u(u,v)$ or $G_r(u,v)$, and $G(u,v)$ is the unknown spectrum. We use as unknown reference spectrum, either the spectrum $G(u,v)$ given in (27) [Fig. 3(b)], or the spectrum $G_0(u,v)$ obtained if the real values of the function were known on the grid. In $G_o(u,v)$ the truncation artifacts due to the finite 64×64 grid are also present. The results are given in Table I. The root sampling method has a better performance for all cases. Similar results were obtained with other functions too.

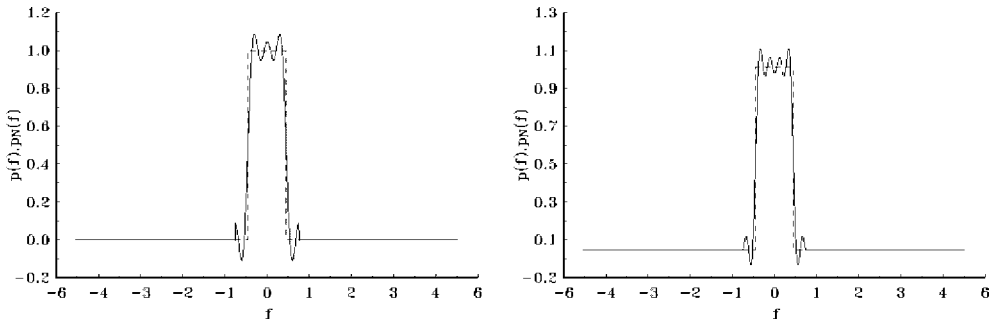

(a) (b)

Fig. 5. (a) The reconstruction (solid line) of a pulse (dashed line) by uniform sampling. (b) The reconstruction (solid line) of a pulse (dashed line) by sampling on the roots of $J_0(r)$.

Then, we examine the immunity of the methods to noise. We add uniform noise in $[-.005, .005]$ to the samples for the case of $N = 32$ circles and $M = 128$ samples/circle. The NRMS signal-to-noise (S/N) ratio of the samples is 18 dB for the uniform sampled data and 16.6 dB for the root sampled data. The S/N of the reconstructed signal compared to spectrum $G_o(u, v)$, is 6.3 dB for the uniform sampling and 9.2. dB for the root sampling. Again root sampling has a better noise performance.

Finally, we examine the mean square error (MSE) of the two sampling schemes for the one-dimensional (1-D) case. It is defined as [11]

$$E_N = \int_{-\infty}^{\infty} |f(t) - f_N(t)|^2 \, dt = \int_{-\infty}^{\infty} |F(\omega) - F_N(\omega)|^2 \, d\omega \quad (28)$$

where $f(t)$ is the given function—sinc (σt)—and $f_N(t)$ the reconstructed one by N samples. For the uniform sampling, $f_N(t)$ is given by [11]

$$f_N(t) = \sum_{n=-N}^{N} f(nT) \, \frac{\sin \sigma(t - nT)}{\sigma(t - nT)} \quad (29)$$

where

$$T = \pi/\sigma. \quad (30)$$

For the root sampling $f_N(t)$ is given by (see, also [7])

$$f_N(t) = \frac{2}{\sigma} \sum_{i=1}^{N} \frac{a_i f(a_i)}{J_1(a_i \sigma)} \, \frac{J_0(\sigma t)}{a_i^2 - t^2} \quad (31)$$

where

$$a_i = x_i/\sigma. \quad (32)$$

Notice that we do not use the sample at $t = 0$.

For the numerical evaluations we used $\sigma = \pi \; r/s, T = 0.6$ s, and N in the interval (3, 20). The resulting error curves are depicted in Fig. 4. The error of the root sampling, for a finite number of samples, is almost the same with that of the uniform sampling. In Fig. 5(a) and (b) the reconstruction of a pulse is illustrated for the two cases $(N = 5)$. It appears that for the same number of samples the root sampling [see Fig. 5(b)] gives a better representation near the discontinuity points.

VII. Discussion and Conclusion

In this essay, we established the polar sampling theorem for sampling on the roots of $J_0(r)$. We derived a new closed formula to reconstruct an arbitrary 2-D bandlimited signal from its values on concentric circles. To date the theorem was applied restrictively to circularly symmetric functions. The extended theorem enables the sampling at the same distances as the uniform sampling, but allows us to calculate the values of the bandlimited function via a closed formula. Moreover, as compared with the uniform polar sampling, the root sampling requires considerably fewer samples for its numerical implementation. If we use the same number of samples for both methods, then polar sampling gives better results, it is less sensitive to noise and in our numerical implementation it requires less computing time.

Appendix

Uniform Sampling Theorem: If the values of the α-bandlimited function $f(r, \theta)$ are known on the concentric circles $f(r = ir_0, \theta), r_0 \leq (\pi/\alpha)$, then the function is known for every r and θ.

Proof: Let r_0 be the radial sampling distance. Each sample along r is located at [Fig. 1(a)]

$$\overline{r} = (r_i, \theta) = (i \cdot r_0, \theta) \qquad i = 0, 1, \cdots, N. \quad (A.1)$$

According to the *central slice theorem* [12], the 1-D FT of a 2-D function along a line passing through the origin and forming an arbitrary angle $\theta = \theta_0$ with the x axis, equals to the projection of the 2-D FT of the function at the same angle $\varphi = \theta_0$. The projection is described by [13]

$$P_{\omega_\varphi}(\omega) = \iint_{u,v} F(u, v) \delta(\omega_\varphi - \omega) \, du \, dv \quad (A.2)$$

where

$$\omega_\varphi = u \cos \varphi + v \sin \varphi \quad (A.3)$$

and u, v are the rectangular coordinates of the Fourier domain.

If the 2-D FT is limited by a maximum radial frequency α, its projections will be restricted by α too

$$P_{\omega_\varphi}(\omega) = 0, \qquad \omega > \alpha.$$

Therefore, if we acquire an infinite number of lines through $f(r, \theta)$ for different θ—covering the entire space (r, θ)—we can in principle reconstruct $f(r, \theta)$ from its samples along these lines. Indeed, imposing a sampling distance $r_0 \leq (\pi/\alpha)$ on each line, we can acquire $f(r, \theta)$ by using the sampling theorem. Hence, the function $f(r, \theta)$ is defined for every r and θ.

Lemma 1: If the nth-order HT $\tilde{g}_n(\omega)$ of a circularly symmetric function $g(r)$ is α-bandlimited, i.e.,

$$g(r) \overset{h_n}{\longleftrightarrow} \tilde{g}_n(\omega) = 0 \qquad \omega > \alpha \quad (A.4)$$

then its zeroth-order HT

$$g(r) \overset{h_0}{\longleftrightarrow} \tilde{g}_0(\omega) = 0 \qquad \omega > \alpha \quad (A.5)$$

is α-bandlimited too.

Note: h_i denotes the ith-order HT

$$g(r) \overset{h_i}{\longleftrightarrow} \tilde{g}_i(\omega) = \int_0^\infty rg(r)J_i(\omega r)\, dr. \tag{A.6}$$

Proof: We form the 2-D function $g(r)e^{jn\theta}$ with 2-D FT [7]

$$h(r,\theta) = g(r)e^{jn\theta} \leftrightarrow H(\omega,\varphi) = \tilde{g}_n(\omega)e^{-jn\varphi} \tag{A.7}$$

where $\tilde{g}_n(\omega)$ is the nth-order HT of $g(r)$, and $H(\omega,\varphi) = 0$ if $\omega > \alpha$.

The line of $h(r,\theta)$ at x-axis ($\theta = 0$) equals to $g(r)$ with 1-D FT

$$h(r,0) = g(r) \leftrightarrow P_{\varphi=0}(\omega) = 0 \qquad \omega > \alpha \quad \text{and} \quad \varphi = 0. \tag{A.8}$$

The latter results from the fact that $\tilde{g}_n(\omega)$ is the amplitude of $H(\omega,\varphi)$ [see (A.7)] and it equals to zero for $\omega > \alpha$, and the same argument is true for its projections $P_{\omega_{\varphi=0}}(\omega)$ on the horizontal axis. We, thus, conclude that $g(r)$ is α-bandlimited.

We form now the circularly symmetric 2-D function $k(r,\theta) = g(r)$ with 2-D FT [7]

$$k(r,\theta) = g(r) \leftrightarrow K(\omega,\varphi) = \tilde{g}_0(\omega). \tag{A.9}$$

From (A.8) each 1-D slice of $k(r,\theta)$ is α-bandlimited and, consequently, each projection of $K(\omega,\varphi)$ is zero for $\omega > \alpha$. Thus according to the *central slice theorem* $\tilde{g}_0(\omega)$ is also α-bandlimited, i.e.,

$$\tilde{g}_0(\omega) = 0 \qquad \omega > \alpha. \tag{A.10}$$

It can be proved that if $\tilde{g}_n(\omega)$ is α-bandlimited, then $\tilde{g}_k(\omega)$ is also α-bandlimited for $k = n-1, \cdots, 0$.

REFERENCES

[1] D. E. Dudgeon and R. M. Mersereau, *Multidimensional Digital Signal Processing.* Englewood Cliffs, NJ: Prentice-Hall, 1984.

[2] G. H. Glover and A. T. Lee, "Motion artifacts in MRI: Comparison of 2DFT with PR and spiral scan methods," *Magn. Reson. Med.*, vol. 33, p. 624, May 1995.

[3] S. Alliney, S. Matej, and I. Bajla, "On the possibility of direct Fourier reconstruction from divergent-beam projections," *IEEE Trans. Med. Imag.*, vol. 12, pp. 173–181, June 1993.

[4] J. Doulgerakis, G. Xerogiannakis, and N. Myridis *et al.*, "The application of the Hankel Transform in MRI. The Optimal Hankel Transform Reconstruction (OHTR)," in *Proc. 12th Annu. Scientific Meeting of the Society of Magnetic Resonance in Medicine*, vol. 2, Aug. 1993, p. 727.

[5] N. Myridis and C. Chamzas, "K-Space sampling: A new trajectory and two reconstruction methods," in *Proc. Society of Magnetic Resonance, 4th Scientific Meeting*, vol. 3, Apr. 27–May 3, 1996, p. 1616.

[6] S. R. Deans, *The Radon Transform and Some of Its Applications.* New York: Wiley, 1983.

[7] A. Papoulis, *Systems and Transforms with Applications in Optics.* New York: McGraw-Hill, 1968.

[8] R. J. Marks II, *Advanced Topics in Shannon Sampling and Interpolation Theory*. New York: Springer-Verlag, 1993.

[9] E. Jahnke and F. Emde, *Tables of Functions with Formulae and Curves.* New York: Dover, 1938.

[10] H. L. Keng, *Introduction to Number Theory*. New York: Springer-Verlag, 1982.

[11] A. Papoulis, *Circuits and Systems.* New York: Holt, Rinehart and Winston, 1980.

[12] A. C. Kak and M. Slaney, *Principles of Computerized Tomographic Imaging.* Piscataway, NJ: IEEE Press, 1988.

[13] A. K. Jain, *Fundamentals of Digital Image Processing.* Englewood Cliffs, NJ: Prentice-Hall, 1989.

Determining Data Independence on a Digitized Membrane in Three Dimensions

Lawrence M. Lifshitz

***Abstract*— A method for determining whether structures distributed along a cell's membrane represent a random spatial distribution is presented in this paper. Two three-dimensional (3-D) images are acquired from one cell by wide-field digital imaging of cells which have been labeled with two different fluorescent antibodies. Prior to spatial analysis, a constrained regularized least squares restoration of the images is performed. This is followed by registration via fiducial markers (dual-labeled beads). A deformable model is then used to map data near the surface to the surface. Finally, each resulting data set is analyzed to determine whether it is spatially random. To do this, we generalize the test for complete spatial randomness of points in a plane, to test voxels distributed along a voxelized membrane in three dimensions. We also test whether the distribution of one protein is independent of the distribution of a second protein. The method is applied to compare the distribution of the protein kinase C to that of vinculin. Vinculin is a protein which anchors intracellular filaments to the cell's plasma membrane. It is also used as a (sparse) membrane marker for the deformable model. Protein kinase C facilitates molecular motors inside the cell. These may be associated with actin and myosin filaments.**

***Index Terms*—Light microscopy, multidimensional data analysis, pattern recognition, spatial statistics.**

I. INTRODUCTION

One the main areas of interest to cell physiologists is the spatial relationship within one type of cell constituent or between two types. To examine these relationships we have designed wide field, charge-coupled device (CCD)-based microscopes which permit the acquisition of dual wavelength three-dimensional (3-D) images of cells. This capability permits the digital imaging of cells which have been labeled with two different fluorescent antibodies (so two types of cell constituents are marked). Thus, two 3-D images are acquired from one cell. Prior to analysis a constrained, regularized (by the square of the image intensity) least squares restoration [1] of the images is performed. This is followed by registration via fiducial markers (dual-labeled beads).

II. BACKGROUND

A. Biological Tasks

The biological application which will be discussed in this paper is the examination of the spatial relationship between protein kinase C (PKC) and vinculin, as well as the distribution of each separately. Vinculin is a protein which anchors intracellular filaments to the cell's plasma membrane. It is used as both a (sparse) membrane marker and to delineate regions of the cell away from the caveoli (where most of the plasma pumps and channels reside). PKC facilitates molecular motors inside the cell. These may be associated with actin and myosin filaments.

Manuscript received March 13, 1997; revised February 27, 1998. This work was supported in part by the National Science Foundation (NSF) under Grant BIR-9200027 and by the National Institutes of Health (NIH) under Grants RR097-99 and HLA7530. The Associate Editor responsible for coordinating the review of this paper and recommending its publication was M. W. Vannier.

The author is with the Biomedical Imaging Group, University of Massachusetts Medical School, 373 Plantation Street, Suite 114, Worcester, MA 01605 USA (e-mail: lml@vision.ummed.edu).

Publisher Item Identifier S 0278-0062(98)04885-X.